

Investigation of annealing temperature on the structural, optical and electrical properties of Sn-doped ZnO thin films by sol–gel method

ZIXUAN LAO, YUEHUI HU*, YICHUAN CHEN, KEYAN HU, WENJUN ZHU, WEIQIANG SHUAI

Department of Mechanical and Electronic Engineering, Jingdezhen Ceramic Institution, Jingdezhen 333403, Jiangxi, China

In this work, tin-doped zinc oxide (TZO) thin films was deposited on quartz glass substrate using a sol-gel technique. The effects of various annealing temperature on structural, optical and electrical properties of the TZO thin films have been investigated by X-ray diffraction (XRD), scanning electron microscopy (SEM), UV-VIS spectrophotometer and Hall effect measurement system, respectively. XRD patterns reveal that all the films have a polycrystalline structure with a preferential orientation along the (002) plane. The crystallite size and lattice parameter values of the thin films was calculated. Calculations showed that the average size of TZO thin films increased from 17.1 to 28.6 nm with increasing annealing temperature from 450 to 600°C. Moreover, the average optical transmittance of the TZO thin films was over 85% in the wavelength range of 300~1000 nm. The optical band gap of TZO thin films increased from 3.193 to 3.256 eV with increasing annealing temperature from 450 to 600°C. Among of the TZO thin films in this work, films annealed at 500°C exhibited the best photoelectric properties, namely average transmittance of 93.2%, a carrier concentration of $2.027 \times 10^{20} \text{cm}^{-3}$ and a resistivity of $6.979 \times 10^{-3} \Omega \cdot \text{cm}$.

(Received April 11, 2017; accepted February 12, 2018)

Keywords: Sol-gel, Sn-doped ZnO, Annealing temperature, Photoelectric properties

1. Introduction

Zinc oxide (ZnO) thin films have got a wide range of concern in the field of wide band gap semiconductors which can be used in photodetectors [1], light-emitting diode [2], thin film transistors [3], perovskite solar cell [4], piezoelectric devices [5], gas sensor [6], diluted magnetic semiconductor and other optoelectronic components [7]. ZnO is an n-type semiconductor material that belongs to II–VI group with a wide band gap of 3.37eV at room temperature [8], and exhibited large exciton binding energy of 60 meV [9]. ZnO based thin films have excellent chemical stability in hydrogen plasma atmosphere, and abundant raw material source [10], low price, these properties makes it has been considered as a hopeful substitute for ITO thin films, and is widely considered to be one of the most promising transparent conducting materials [11]. The conductivity of undoped ZnO thin films are unsatisfactory in commercial due to the intrinsic defect oxygen vacancies and zinc interstitial, so that the undoped ZnO cannot be used for thin films solar cell contact layer directly and pure ZnO thin films are not stable due to changes in the surface conductance under oxygen chemisorptions and adsorptions [12]. Therefore, doped ZnO films have attracted great interest such as doped with Na^{1+} , Ag^{1+} , Mg^{2+} , B^{3+} , Al^{3+} , Ga^{3+} , In^{3+} and

Sn^{4+} [13]. Among these dopants, the main reason of being chosen of Sn as the dopant in ZnO is ionic radius of Sn^{4+} (0.69 Å) is similar to Zn^{2+} (0.74 Å), and thus Sn^{4+} can replace Zn^{2+} in substitutional sites easily [14]. Sn^{4+} substitutes Zn^{2+} site in the ZnO crystal structure releases two more free electrons into the conduction band to enhance the electrical conductivity. Chien-Yie Tsay et al. [15] deposited $\text{Zn}_{2(1-x)}\text{Sn}_x\text{O}_2$ ($x=0.0, 0.01, 0.02, 0.03, 0.05$) thin films using sol-gel method and investigated effect of dopants on the crystallinity, microstructural and optical properties. They reported that the 2 at.% Sn-doped ZnO thin film exhibited the smoothest surface morphology, the best average transparency of 90% and the resistivity of $9.3 \times 10^{-2} \Omega \cdot \text{cm}$. F. Z. Bedia et al. [16] produced Sn-doped ZnO thin films with 0, 0.5, 1, 1.5 and 2 at.% Sn by spray pyrolysis method and reported that the films consist of hexagonal-like grains. Yasemin Caglar et al. [17] synthesized Sn-doped ZnO thin films with 0, 1, 3 and 5 at.% Sn by spray pyrolysis method and effect of Sn dopant on the structural and morphological properties of these films was investigated. According to this report, Sn-doped ZnO thin films had a c-axis orientation of the wurtzite structure. The crystallite size increases initially with the increase of Sn content and reaches a maximum value of 42 nm. In summary, all of these works are only investigated the effect of the concentration of Sn on the properties of

the films.

Sn-doped ZnO thin films can be deposited by several methods such as radio frequency magnetron sputtering [18], Hydrothermal method, pulsed laser deposition (PLD) [19], electron beam evaporation method, metal-organic chemical vapor deposition (MOCVD) [20], and sol-gel method [21]. Among them, sol-gel spin coating method is considered to be one of the most effective techniques due to its features such as excellent controllability, low manufacture cost and can be depositing on quartz glass substrate in large area [22]. The sol-gel technique involves several technological parameters for instance the concentration of precursor and its nature, spin coating speeds, preheating time and temperature, the nature of the substrate, annealing time and temperature which will be directly or indirectly affect the performance of ZnO thin films. Among these parameters, the annealing parameters play an important role in the properties of the films. It is necessary for the thin film to be annealed is due to that unannealed thin film can hardly crystallize. However, the effects of annealing temperature on the properties of the Sn-doped thin films are rarely reported. In order to obtain high quality Sn-doped thin films, it demands a pointedly study of the annealing temperature and the technological parameters of spin coating.

2. Experimental

Sn-doped ZnO (TZO) thin films were prepared on quartz glass substrates using sol-gel spin coating method. Zinc acetate dehydrate ($\text{Zn}(\text{CH}_3\text{COO})_2 \cdot 2\text{H}_2\text{O}$) and Tin chloride pentahydrate ($\text{SnCl}_4 \cdot 5\text{H}_2\text{O}$) were used as sol precursor and dopant, Ethanol ($\text{C}_2\text{H}_5\text{OH}$) and Monoethanolamine (MEA) was used as solvent and stabilizer, respectively. Firstly, Zinc acetate dehydrate was dissolved in a mixture of Ethanol, then MEA was added to zinc acetate to obtain sols with 2 at% concentrations. Tin doping was carry out by adding Tin chloride pentahydrate ($\text{SnCl}_4 \cdot 5\text{H}_2\text{O}$) to the precursor solution and Sn/Zn ratios is 2.0 at.%. The solutions of Sn-doped ZnO films was stirred at 60°C for 120 min to obtain a clear and homogenous solution. The obtained solution was aged at room temperature for 48 h before coating. TZO thin films were dropped onto pre-cleaned quartz substrates and spin at rotation speed of 1500 rpm for 10s first and then at 3000rpm for 20s. Afterwards the films were dried at 300°C for 8 min in air ambient condition to evaporate the solvent and organic residues. After the above steps were repeated six times, these samples were then put into a rapid annealing furnace and annealed in argon at 450°C , 500°C , 550°C and 600°C for 15 min which were labeled as 1#, 2#, 3#, 4#, respectively. The whole annealing process includes rapid heating, thermal insulation and natural cooling. The experimental flowchart and annealing process are shown in Fig. 1 and Fig. 2.

The prepared thin films were subjected by X-ray diffraction (XRD) using X-ray diffractometer ($\lambda=1.54 \text{ \AA}$,

Rigaku D/Max-2500PC) with the radiation of Cu K α which is operated at 40 kV and 30 mA from 20° to 70° , and the speed of scanning was $2^\circ/\text{min}$ for calculate structure parameters such as crystallite size, dislocation density and lattice parameters. SEM (QuanTA-200F) was used to observed the surface morphology of the as-prepared samples. The transmittance (T) were measured by the ultraviolet-visible spectrometer (PerkinElmer, Lambda 950) over the wavelength range from 300 to 1000 nm. The data was recorded at room temperature and all the optical parameters such as absorption coefficient α , optical band gap E_g . The electrical properties of thin films were analyzed by Hall effect measurement system (SWIN, Hall 8800). All the measurements were obtained at room temperature.

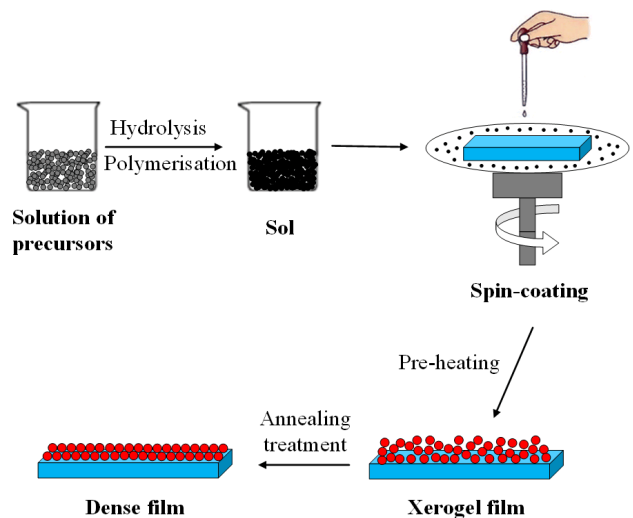


Fig. 1. The experimental flowchart of TZO thin films prepared by sol-gel method

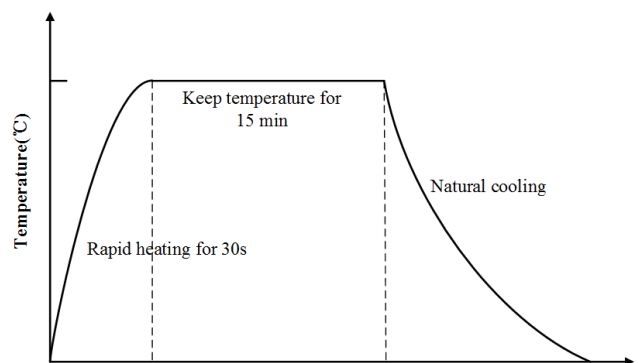


Fig. 2. The annealing process of TZO thin films

3. Results and discussion

Fig. 3 shows X-ray Diffraction (XRD) patterns of TZO thin films with various annealing temperatures. The observed peaks for the nanorod arrays are attributed to a polycrystalline structure with hexagonal wurtzite structure films (zincite phase JCPDS # 36-1451) and exhibit a

preferred (002) orientation. A broad peak in the vicinity of 22° occur for all the prepared TZO thin films, which are the intrinsic diffraction peak of the quartz substrate. The intensity of the (002) peaks exhibits a dominant diffraction, thus, the films are preferentially oriented along the c-axis and perpendicular to the substrate surface. The diffraction angle of (002) peaks shifted towards lower angles first and then shifted towards higher angles by increasing the annealing temperature, implying that the lattice constant 'c' changed for all TZO thin films. These performances were mainly caused by intrinsic stress of TZO thin films. The intensity of (002) peaks was raised with the increasing annealing temperature, which is means that the TZO thin films were further crystallized with the increase of annealing temperature. The pores and defects between grains decreased, thus the microstructure of thin films become more ideally. The diffraction peak of the thin film is the most intense at the temperature of 600°C that can be attributed to thin films occurs second times of recrystallization to promote the readjust of microstructure at high temperature.

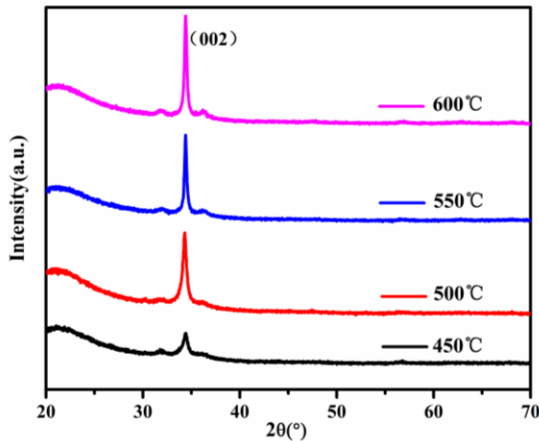


Fig. 3. XRD spectra of TZO thin films annealed under different annealing temperature

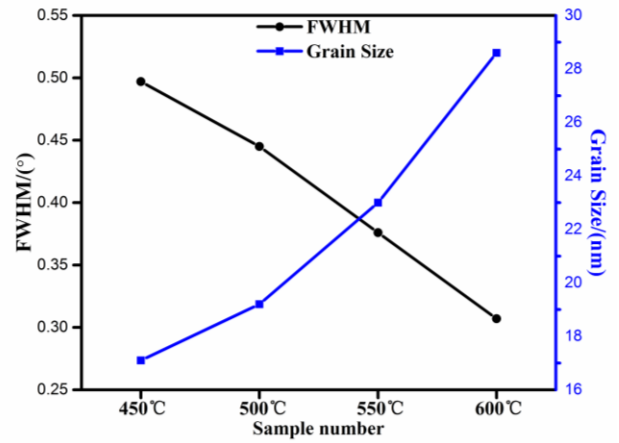


Fig. 4. Relationship between the half height width and grain size of TZO thin films under different annealing temperature

The lattice constants 'a' and 'c' of TZO thin films with (002) orientations are calculated by the following relations [23]:

$$a = \frac{\lambda}{\sqrt{3} \sin \theta}$$

$$c = \frac{\lambda}{\sin \theta}$$

The volume (V) of the unit cell and the Zn-O bond length (L) has been calculated using:

$$V = \frac{\sqrt{3}}{2} \times a^2 \times c$$

$$L = \sqrt{\frac{a^2}{3} + \left(\frac{1}{2} - u\right)^2 c^2}$$

$$\text{Where } u = \left(\frac{a^2}{3c^2}\right) + 0.25$$

The average grain size (D) of the films was calculated using the full width at half maximum (FWHM) of (002) peak from the Scherrer' s formula [24]:

$$D = \frac{k\lambda}{\beta \cos \theta}$$

Table 1. Structural parameters of (002) diffraction peak of TZO thin films under different annealing temperature

Sample	Lattice parameters		Volume of unit cell (\AA^3)	2θ (deg)	FWHM β (deg)	Average crystallite size (D) (nm)	Zn-O bond length(\AA)
	a(\AA)	c (\AA)					
1#	3.0032	5.2017	40.629	34.442	0.497	17.1	1.8784
2#	3.0132	5.2190	41.036	34.324	0.445	19.2	1.8846
3#	3.0069	5.2073	40.684	34.398	0.376	23.0	1.8790
4#	3.0064	5.1960	40.760	34.404	0.307	28.6	1.8804

Where $K=0.89$ is the Scherrer constant, λ is wavelength of incident X-ray, β is the full width at half-maximum (FWHM) measured in radians and θ is the Bragg angle of diffraction peak [25]. Table 1 shows Structural parameters of (002) diffraction peak of TZO thin films under different annealing temperature. As the Table 1 shows, the a -axis lattice constants and c -axis constants were increased first and then decreased. The average grain size of the samples was 17.1 nm, 19.2 nm, 23.0 nm and 28.6 nm, respectively. It is observed from Fig. 4 that, the FWHM value of (002) peaks exhibited a tendency to decrease as the annealing temperature is raised, this phenomenon and the previous XRD results demonstrated that the crystallinity of the thin films increased with the increase of annealing temperature.

It was also observed that crystallite size increased with increasing annealing temperature for the TZO thin films. This is mainly due to the annealing process induced the small grains merged together by grain boundary diffusion, which leads to growth of the major grains. The grain growth principle involves the transfer of atoms from one grain to another at grain boundaries, and the annealing treatment determined the final grain size.

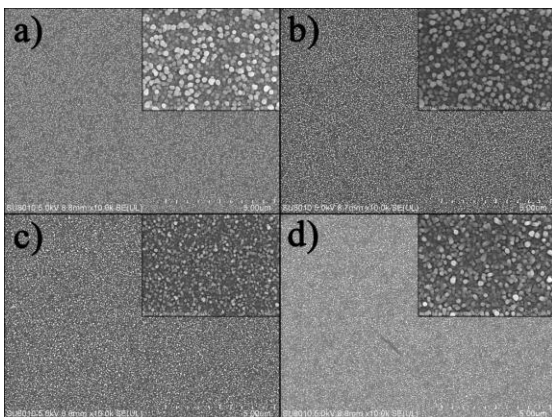


Fig. 5. SEM image of TZO thin films under different annealing temperature: a) 450°C; b) 500°C; c) 550°C; d) 600°C

Fig. 5 shows the surface morphology of the TZO thin films with different annealing treatment. It is revealed that the nanostructure of the TZO thin films for spin coating with an average grain size of 17 to 28 nm with annealing temperature from 450 to 600°C, respectively. We can learn from the SEM micrographs that all of TZO thin films are polycrystalline structures (no pores are observed). It can be seen from the figure that the thin films annealed at high temperature have uniform grain size and orderly distribution. In addition, the grain shows an obvious columnar shape which is a typical hexagonal wurtzite structure of ZnO. This result is consistent with the previous XRD analysis. The

sample shows obvious structure of nanorods and perpendicular to substrate surface at the temperature of 600°C. The result shows that in a certain temperature range, the higher annealing temperature is easier to form a better film.

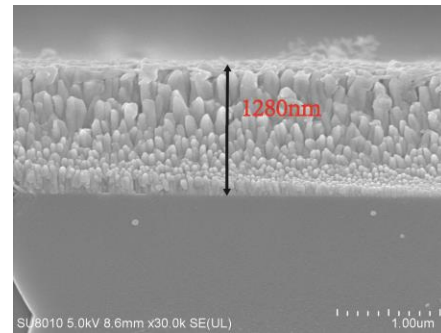


Fig. 6. A cross-sectional SEM image of TZO thin films

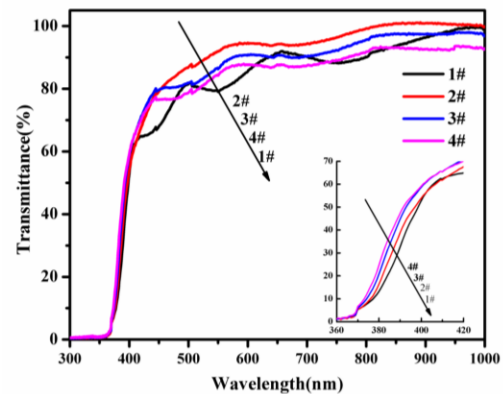


Fig. 7. Transmittance spectra of TZO thin films under different annealing temperature

A cross-sectional SEM image and optical transmittance spectra of the TZO thin films are shown in Fig. 6 and Fig. 7. The thickness of TZO thin films was 1280 nm. The average transmittance of TZO thin films annealed at 450°C, 500°C, 550°C and 600°C were 87.2%, 93.2%, 90.1%, and 86.7%, respectively. It can be observed from the figure that as the annealing temperature increases, the transmittance of the thin films tends to increase first and decreased after. At first, When the annealing temperature increased from 450°C to 500°C, the transmittance of the thin film reached 93.2%. Then the transmittance of the thin films gradually decreased when the annealing temperature rises again. It could be explained by the grains size in samples growth by increase of annealing temperature, and the grain boundary diffusion which resulted in the scattering of light decreases. As the samples were annealed under even higher temperature, the thin films occurred second times of recrystallization to promote the reorganization of microstructure, which leads to the thickness of the thin film have changed (Fig. 5), thus results in the

decrease of the thin films transmittance. All samples exhibit sharp ultraviolet absorption edges at about $\lambda \approx 370$ nm. These absorption edges obviously depend on the annealing temperature and the atmosphere of annealing. The inset of Fig. 7 shows that 2#, 3#, 4# thin films appeared blue-shift absorption edge in comparison to the 1# sample. The optical band gap was determined by Tauc method. First, the absorption coefficient, α was calculated using the following equation [26]:

$$\alpha = \frac{\ln(1/T)}{D}$$

Where the normalized optical transmittance, T was obtained from optical transmittance spectra, which has been normalized to the highest measured value by setting it to 100%. D is the thin film thickness measured by surface profilometer.

The optical band gap for direct band semiconductor was then estimated with the following equation [27]:

$$(\alpha h\nu)^2 = A(h\nu - E_g)$$

Where A is a constant, $h\nu$ is the energy of incident photon and E_g is the optical band gap. The optical band gap energies E_g are calculated by plotting Tauc's graphs between $(\alpha h\nu)^2$ versus photon energy $h\nu$ and the intercept of this linear region on the energy axis at $(\alpha h\nu)^2$ equal to zero gives the optical band gap of deposited thin films. The plot of $(\alpha h\nu)^2$ against $h\nu$ presents a linear relationship. Which means that TZO thin films are direct transition type semiconductor. Fig. 8 shows the dependence of E_g on temperature, and the band gap of samples increases from 3.193 eV to 3.256 eV with temperature raised from 450°C to 600°C, it could be attributed to the Fermi level raises into the conduction band by the Burstein-Moss effect. The intrinsic absorption edge shifts to the short-wave direction that is blue-shift absorption edge, known as the Burstein-Moss shift[28]. As the annealing temperature increases, the carrier concentration also increases, leading to low levels is filled in the conduction band, this result in a broadening of the optical band gap.

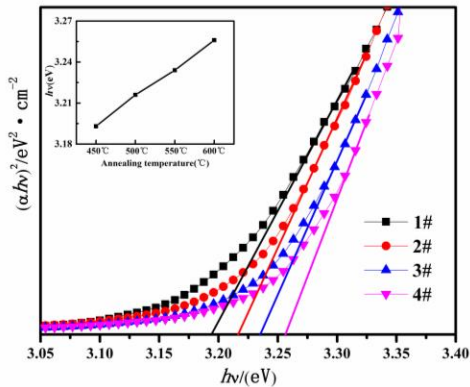


Fig. 8. The relationship of $(\alpha h\nu)^2$ - $h\nu$ TZO thin films under different annealing temperature

The electrical properties of the TZO thin films are mainly determined by the carrier concentration and the carrier mobility in the thin films. The carrier concentration is mainly derived from the hole, electron and the intrinsic defects in the thin films. The resistivity of TZO thin films is obviously lower than that of undoped ZnO films due to the position of Sn^{4+} ions instead of sites of Zn^{2+} ions. The substituted Sn atoms can be ionized easier than zinc atoms because of their lower ionization potential. The electrical properties of the samples annealed at different temperatures are shown in Fig. 9, including resistivity, carrier concentration, and carrier mobility. We can found that as the annealing temperature increased to 500°C, the resistivity directly decreased to the minimum value of $6.979 \times 10^{-3} \Omega \cdot \text{cm}$ and the carrier concentration is the highest. The possible reason is that the annealing process has the effect of increasing grain size and crystallinity of the thin film, as mentioned before, with the increase of temperature in a certain range which therefore results in less grain boundary scattering and improve the carrier concentration and lifetime. On the other hand, loss of oxygen from the crystal will produce the interstitial zinc atoms, as well as conducive to the adsorption of oxygen in grain boundary be decomposed which results in increases oxygen vacancies. Oxygen vacancies can be a positive center and attracting negative coulomb. The conduction band moving towards the low level forming a donor level, leads to the increase of carrier concentration. However, when the annealing temperature rises from 550°C to 600°C, the resistivity gradually increased which is caused by the grain size grew up to much so that carrier mobility decreased. Experimental investigation shows that the conductivity of TZO is the best at the temperature of 500°C.

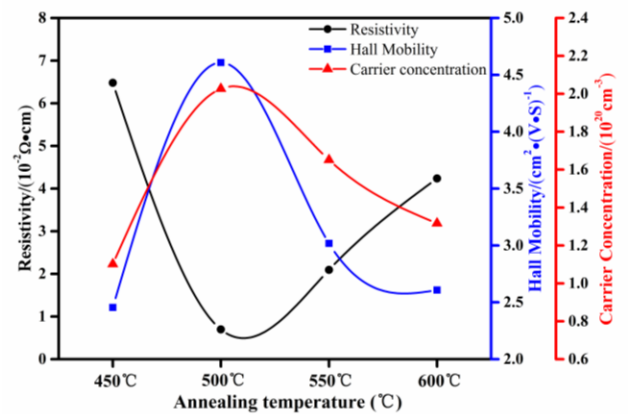


Fig. 9. Resistivity spectra of TZO thin films under different annealing temperature

4. Conclusion

In this work, the effect of annealing temperature on structural, electrical and optical properties of TZO thin

films prepared via sol-gel method was investigated in argon ambient. This study has proved that the annealing temperature plays an important role in modifying the structural and photoelectric characteristics of the TZO thin films. Our result reveals that an increase in the grain size of TZO thin films with increasing annealing temperature from 450°C to 600°C. The annealing temperature also has an obvious effect on the optical transmittance and electric conductivity of TZO thin films. A highly transparent conductive thin film with a transmittance of 93.2% and a resistivity of $6.979 \times 10^{-3} \Omega \cdot \text{cm}$ was fabricated at an annealing temperature of 500°C. This could be the optimum annealing temperature for TZO thin films which can be used in transparent conductive oxide thin film on glass and plastic substrates.

Acknowledgments

This work was financially supported by the following funds: (1) The Natural Science Foundation of China (No.61464005); (2) The Natural Science Foundation of Jiangxi Province(No.20143ACB21004, 20151BAB202010 and 20171BAB216015); (3) The Key Research and Development Project of Department of Science and Technology of Jiangxi Province (No.20171BBE52053); (4) The Jiangxi Province Foreign Cooperation Projects (No. 20151BDH80031); (5) The College Students Innovation and Entrepreneurship Training Program of Jingdezhen Ceramic Intitute (No.212050-008).

References

- [1] A. Amala Rani, Suhashini Ernest, Superlattices and Microstructures **75**, 398 (2014).
- [2] H. Aydin, H. M. El-Nasser, C. Aydin, Ahmed A. Al-Ghamdi, F. Yakuphanoglu, Applied Surface Science **350**, 109 (2015).
- [3] M. Bouderbala, S. Hamzaoui, M. Adnane, T. Sahraoui, M. Zerdali, Thin Solid Films **517**(5), 1572 (2009).
- [4] Lin Cui, Gui-Gen Wang, Hua-Yu Zhang, Rui Sun, Xu-Ping Kuang, Jie-Cai Han, Ceramics International **39**(3), 3261 (2013).
- [5] Ian Y. Y. Bu, Materials Science in Semiconductor Processing **27**, 19 (2014).
- [6] Mujdat Caglar, Yasemin Caglar, Seval Aksoy, Saliha Ilican, Applied Surface Science **256**(16), 4966 (2010).
- [7] Reza Ebrahimifard, Mohammad Reza Golobostanfard, Hossein Abdizadeh, Applied Surface Science **290**, 252 (2014).
- [8] J. B. You, X. W. Zhang, Y. M. Fan, Z. G Yin, P. F. Cai, N. F. Chen, Applied Surface Science **255**(11), 5876 (2009).
- [9] P. Periyat, S. G Ullattil, Materials Science in Semiconductor Processing **31**, 139 (2015).
- [10] Yuehui Hu, Yichuan Chen, Jun Chen, Xinhua Chen, Defu Ma, Applied Physics A **114**(3), 875 (2013).
- [11] Dongyu Fang, Kui Lin, Tao Xue, Can Cui, Xiaoping Chen, Pei Yao, Huijun Li, Journal of Alloys and Compounds **589**, 346 (2014).
- [12] K. Khojier, H. Savaloni, E. Amani, Applied Surface Science **289**, 564 (2014).
- [13] H. Mahdhi, Z. Ben Ayadi, S. Alaya, J. L. Gauffier, K. Djessas, Superlattices and Microstructures **72**, 60 (2014).
- [14] Mejda Ajili, Michel Castagné, Najoua Kamoun Turki, Superlattices and Microstructures **53**, 213 (2013).
- [15] Chien-Ye Tsay, Hua-Chi Cheng, Yen-Ting Tung, Wei-Hsing Tuan, Chung-Kwei Lin, Thin Solid Films **517** (3), 1032 (2008).
- [16] Zhanchang Pan, Xinlong Tian, Shoukun Wu, Chumin Xiao, Zhuliang Li, Jianfeng Deng, Guanghui Hu, Zhigang Wei, Superlattices and Microstructures **54**, 107 (2013).
- [17] Yasemin Caglar, Seval Aksoy, Saliha Ilican, Mujdat Caglar, Superlattices and Microstructures **46** (3), 469 (2009).
- [18] Kyung-Jun Ahn, Ji-Hyeon Park, Beom-Ki Shin, Woong Lee, Geun Young Yeom, Jae-Min Myoung, Applied Surface Science **271**, 216 (2013).
- [19] P. F. Cai, J. B. You, X. W. Zhang, J. J. Dong, X. L. Yang, Z. G Yin, N. F. Chen, Journal of Applied Physics **105**(8), 083713 (2009).
- [20] Ha-Rim An, Hyo-Jin Ahn, Jeong-Woo Park, Ceramics International **41**(2), 2253 (2015).
- [21] A. Chelouche, D. Djouadi, H. Merzouk, A. Aksas, Applied Physics A **115**(2), 613 (2013).
- [22] Shuyuan Zhang, Quanxi Cao, Materials Science in Semiconductor Processing **16**(6), 1447 (2013).
- [23] Prakash Chand, Anurag Gaur, Ashavani Kumar, Umesh Kumar Gaur, Ceramics International **40**(8), 11915 (2014).
- [24] Jia Li, Jin-Hua Huang, Yu-Long Zhang, Ye Yang, Wei-Jie Song, Xiao-Min Li, Journal of Electroceramics **26**(1-4), 84 (2011).
- [25] F. Wang, M. Z. Wu, Y. Y. Wang, Y. M. Yu, X. M. Wu, L. J. Zhuge, Vacuum **89**, 127 (2013).
- [26] Saliha Ilican, Mujdat Caglar, Yasemin Caglar, Applied Surface Science **256**(23), 7204 (2010).
- [27] Firoz Khan, Sadia Ameen, Minwu Song, Mushahid Husain, Abdul Mobin, Hyung Shik Shin, Metals and Materials International **19**(2), 245 (2013).
- [28] K. Chongsri, W. Pecharapa, Energy Procedia **56**, 554 (2014).